ISSN (Print) 1226-1750
ISSN (Online) 2233-6656
Journal of Magnetics 17(4), 265-270 (2012) http://dx.doi.org/10.4283/JMAG.2012.17.4.265

Enhanced Low-field Magnetoresistance of $La_{0.7}Sr_{0.3}Mn_{1+d}O_3$-$Mn_3O_4$ Composite Films Prepared by *ex-situ* Solid Phase Crystallization

Young-Min Kang, Hyo-Jin Kim, and Sang-Im Yoo*

Department of Materials Science and Engineering, Seoul National University, Research Institute of Advanced Materials (RIAM), Seoul 151-744, Korea

(Received 6 November 2012, Received in final form 13 December 2012, Accepted 17 December 2012)

We report improved low-field magnetoresistance (LFMR) effects of the $La_{0.7}Sr_{0.3}Mn_{1+d}O_3$-$Mn_3O_4$ composite films with the nominal composition of $La_{0.7}Sr_{0.3}MnO_3$(LSMO)-50 mol% Mn_3O_4. The composite films were fabricated by *ex-situ* solid phase crystallization (SPC) of amorphous films at the annealing temperature region of 900-1100°C for 2 h in a pure oxygen atmosphere. The amorphous films were deposited on polycrystalline $BaZrO_3$ (*poly*-BZO) substrates by dc-magnetron sputtering at room temperature. The Curie temperatures (T_C) of all composite films were insignificantly altered in the range of 368-372 K. The highest LFMR value of 1.29 % in 0.5 kOe with the maximum dMR/dH value of 37.4%kOe^{-1} at 300 K was obtained from 900 nm-thick composite film annealed at 1100°C. The improved LFMR properties of the composite films are attributed to effective spin-dependent scattering at the $La_{0.7}Sr_{0.3}Mn_{1+d}O_3$ grain boundaries sharpened by adjacent chemically compatible Mn_3O_4 grains.

Keywords : low-field magnetoresistance (LFMR), $La_{0.7}Sr_{0.3}MnO_3$ (LSMO)-Mn_3O_4 composite film, dc-magnetron sputtering, solid phase crystallization, spin-dependent scattering

1. Introduction

In the past decades, the discovery of the colossal magnetoresistance (CMR) in doped manganese perovskites, $RE_{1-x}M_xMnO_3$ (RE = rare earth, M = Ca, Sr, Ba, Pb) has drawn much attention of researchers on their fundamental physics and potential applications [1-6]. Among these ferromagnetic manganese perovskites, the LSMO compound with the composition of $La_{0.7}Sr_{0.3}MnO_3$ is known to have the highest T_C of ~370 K and thus regarded as an attractive material for real applications at room temperature. However, since its CMR response occurs in high magnetic fields over 1 T, its practical applications must be very limited.

On the other hand, this compound also shows a significant MR effect in low fields below several kOe, known as the LFMR effect. Interestingly, the LFMR effect is observed only in polycrystalline LSMO samples but not in single LSMO crystals or epitaxial films, implying that high angle grain boundaries of randomly oriented LSMO grains are essential to obtain the LFMR effect. The LFMR effect is attributed to a significant variation in the transport capability of spin-polarized electrons across the LSMO grain boundaries under low magnetic fields [7]. Unfortunately, the LFMR values of the CMR manganites rapidly decrease with increasing temperature and thus become very small at room temperature. The rapid degradation of the LFMR effect with increasing temperature is intimately related to the magnetism of grain boundary which is significantly different from that of grain [8-11] because the grain boundary can act as not only spin-dependent scattering centers but also the spin-flipping centers degrading the LFMR effect. Therefore, for the enhancement of the LFMR effect, it is very critical to control the grain boundary properties of LSMO polycrystalline samples. As such an effort, many groups have attempted to improve the LFMR effect of manganese perovskites by making a composite with insulating oxides [12-18]. The insulating oxides usually hinder the magnetic spin alignment near the grain boundary of manganese perovskites.

Recently, the enhanced LFMR effects in the LSMO-insulating oxide composite films have also been reported in the literature [19-26]. However, reported LFMR values of the composite films were less that 1% at room temperature and thus insufficient for real applications, which

*Corresponding author: Tel: +82-2-880-5720
Fax: +82-2-887-6388, e-mail: siyoo@snu.ac.kr

motivated present study. To enhance the LFMR effect, we investigated the LFMR effects of $La_{0.7}Sr_{0.3}Mn_{1+d}O_3$-$Mn_3O_4$ composite films deposited on *poly*-BZO substrates. As reported in our previous paper for $La_{0.7}Sr_{0.3}Mn_{1+d}O_3$-manganese oxide composite bulks [13], the Mn_3O_4 phase was selected as the secondary phase since it is chemically compatible with the $La_{0.7}Sr_{0.3}Mn_{1+d}O_3$ phase [27].

2. Experimental

The polycrystalline $La_{0.7}Sr_{0.3}Mn_{1+d}O_3$-$Mn_3O_4$ composite films of 900 nm thickness were prepared by *ex-situ* SPC process of amorphous films deposited by dc-magnetron sputtering method [28, 29]. As the first step, an amorphous film was produced by dc-magnetron sputtering of a polycrystalline composite target on polycrystalline *poly*-BZO substrates at room temperature. The 2-inch diameter target with the nominal composition of $La_{0.7}Sr_{0.3}MnO_3$-50 mol% Mn_3O_4 were prepared by the conventional solid-state reaction method using raw materials of La_2O_3, $SrCO_3$ and Mn_2O_3 powders with all 99.9% purity. For the preparation of the *poly*-BZO substrates, the BZO phase was synthesized from the raw materials of $BaCO_3$ (99.9%) and ZrO_2 (99.9%), then the *poly*-BZO bulk samples were prepared by solid state reaction of as-prepared BZO powder at the sintering temperature of 1600°C in air, and finally the bulk *poly*-BZO samples were mechanically thinned (~2 mm in thickness) and surface-polished. The base pressure in the vacuum chamber was maintained at 3×10^{-6} Torr, and the dc power of 75 W was used. The film deposition rate was ~10 nm/min. As the second step, as-deposited amorphous films were crystallized into the composite films by *ex-situ* annealing. *Ex-situ* annealing of amorphous films was performed at high temperatures ranging from 900 to 1100°C for 2 h in pure oxygen gas, and then annealed samples were slowly cooled to room temperature with a cooling rate of 2°C/min.

Phase analysis was performed by XRD (M18XHF-SRA, Mac Science). Microstructure was analyzed by scanning electron microscopy (SEM) (JSM-6330F, JEOL) and transmission electron microscopy (TEM) (F20, FEI). Compositional analysis for the annealed films was performed by STEM (scanning transmission electron microscopy) with EDS (Energy Dispersive X-ray Spectroscopy). Temperature and field dependencies of magnetism were measurement with a superconducting quantum interference device (SQUID) magnetometer (MPMS XL5, Quantum Design). The magnetization versus temperature (*M-T*) curves were measured with zero field-cooled warming procedure in the field of 1 kOe applied parallel to the film plane. The magnetic field was also applied parallel to the film plane for the measurement of magnetization versus magnetic field (*M-H*) curves. The transport measurements for the evaluation of the LFMR effect were performed using the standard four probe method within the SQUID magnetometer, where both the electrical current and magnetic field were applied along the long dimension of samples. The T_C values of the composite films were determined by an extrapolation of ferromagnetic magnetization curves to the temperature axis of zero magnetization value.

3. Results and Discussion

Fig. 1 shows the XRD patterns of the composite films. Both $La_{0.7}Sr_{0.3}Mn_{1+d}O_3$ and Mn_3O_4 peak intensities of the composite films are increased with increasing the annealing temperature (T_{an}), suggesting that their crystallinity becomes improved. According to the La_2O_3-Mn_2O_3 binary phase diagram [27], tetragonal (T)-Mn_3O_4 phase is stable between ~880 and ~1160°C in air and hence it should transform to the Mn_2O_3 phase during slow cooling to room temperature with the cooling rate of 2°C/min in pure oxygen atmosphere. However, the manganese oxides of the composite films commonly exhibit the T-Mn_3O_4 phase due to a strong suppression of the phase transition by adjacent $La_{0.7}Sr_{0.3}Mn_{1+d}O_3$ phase within the composite films, which has also been observed in the $La_{0.7}Sr_{0.3}Mn_{1+d}O_3$-manganese oxide composite bulks with the same nominal composition in our previous study [13].

SEM micrographs of the composite film annealed at 1000°C are represented in the Fig. 2. In the low magnification image of Fig. 2(a), the composite film shows many micro-cracks, which might be generated by a large volume change during crystallization from the amorphous

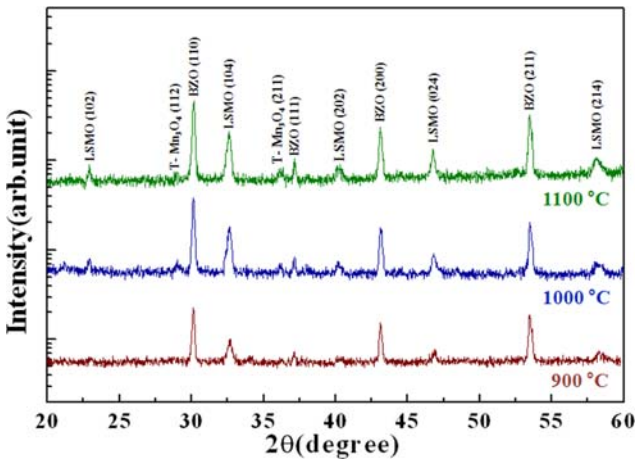

Fig. 1. (Color online) Semi-logarithmic plots for the XRD patterns of the $La_{0.7}Sr_{0.3}Mn_{1+d}O_3$-$Mn_3O_4$ composite films annealed at the temperature region of 900-1100°C.

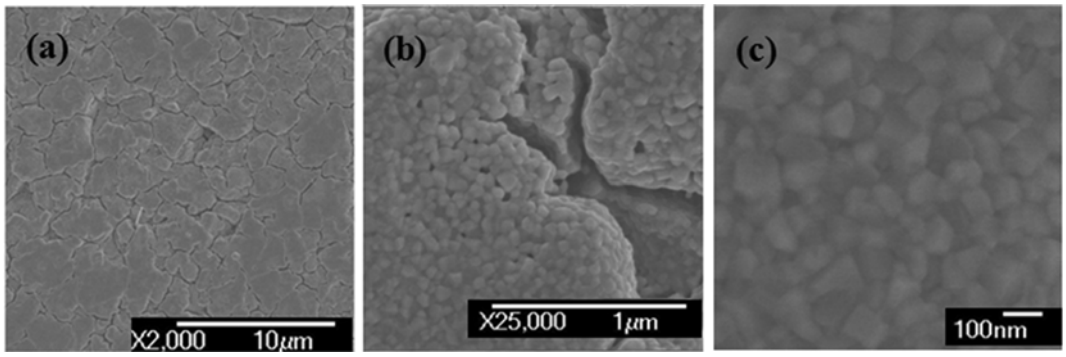

Fig. 2. SEM micrographs of the $La_{0.7}Sr_{0.3}Mn_{1+d}O_3$-$Mn_3O_4$ composite film annealed at 1000°C: (a) low magnification image, (b) image around a gap, and (c) high magnification image.

film. Fig. 2(b) shows a magnified image around a large cleavage gap within the composite film. It can be observed that the composite film is also deposited on the large cleavage gap and thus connected to each other although the film thickness becomes very thin in the gap region. The grain morphologies of $La_{0.7}Sr_{0.3}Mn_{1+d}O_3$ and T-Mn_3O_4 are shown in Fig. 2(c), where the contrast of the $La_{0.7}Sr_{0.3}Mn_{1+d}O_3$ phase is slightly brighter than that of the T-Mn_3O_4 phase. The $La_{0.7}Sr_{0.3}Mn_{1+d}O_3$ phase is composed of equiaxed grains with the average grain size of ~100 nm.

The TEM analysis results for the composite film annealed at 1100°C are shown in the Fig. 3. Fig. 3(a) shows a cross-sectional STEM Z-contrast image of the film. The

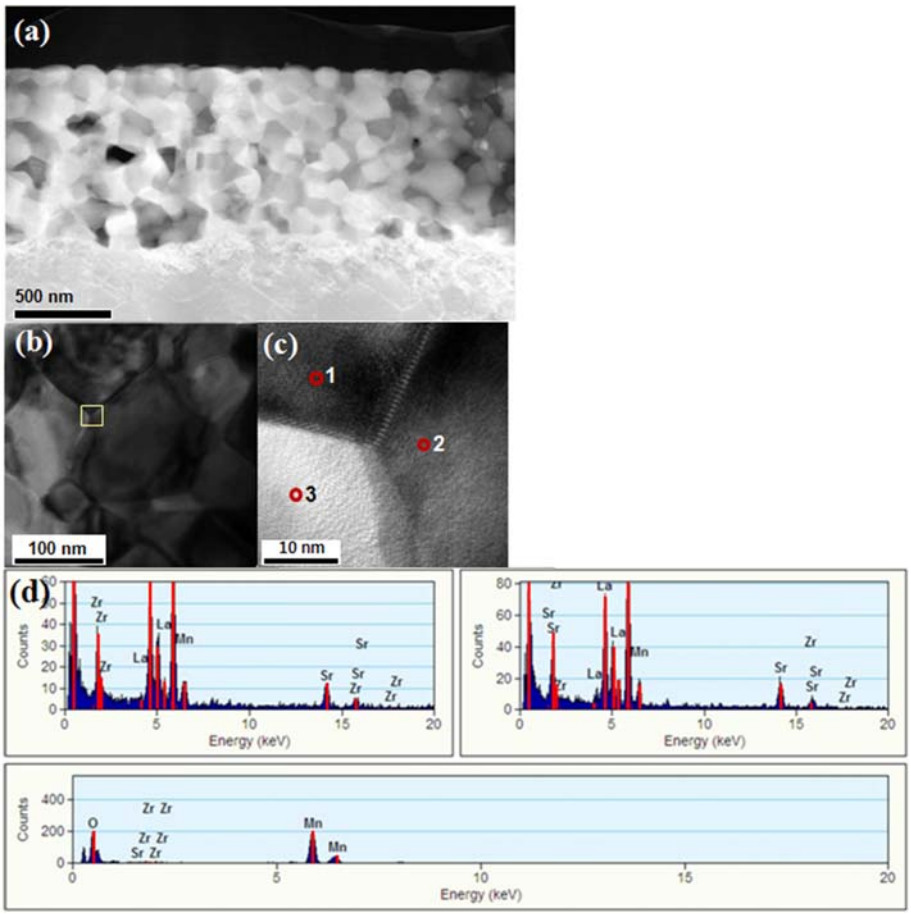

Fig. 3. (Color online) (a) Cross-sectional STEM Z-contrast image of the $La_{0.7}Sr_{0.3}Mn_{1+d}O_3$-$Mn_3O_4$ composite film annealed at 1100°C, (b) its local magnified image, (c) HR-TEM image around a triple grain boundary indicated as a square line in (b), and (d) EDS analysis results corresponding to the three points of 1, 2, and 3 each grain in (c).

morphologies of $La_{0.7}Sr_{0.3}Mn_{1+d}O_3$ and Mn_3O_4 grains are clearly observed as bright and HR-TEM images in Fig. 3(b) and (c), respectively. Fig. 3(c) shows the HR-TEM image of a triple grain boundary junction, corresponding to the square region marked in Fig. 3(b). To identify each phase of the composite film in Fig. 3(c), the EDS analyses were performed on the three points of 1, 2 and 3 in each grain. The EDS data are represented in Fig. 3(d). From the analysis of these data, it was confirmed that two grains corresponding to the points 1 and 2 were the $La_{0.7}Sr_{0.3}Mn_{1+d}O_3$ phase, and one grain corresponding to the point 3 was the T-Mn_3O_4 phase.

Fig. 4 shows the *M-T* curves of the composite films. The magnetization values are increased with increasing T_{an}, which is most probably due to improved crystallinity as previously mentioned on the basis of XRD patterns in Fig. 1. The T_C values of the composite films are insignificantly varied in the range of 369-372 K as listed in the Table 1. Another magnetic transition observed at ~43 K in the composite samples is originated from the ferrimagnetic to paramagnetic transition of the T-Mn_3O_4 phase which was first reported by Borovick-Romanov and Orlova [30].

The *M-H* curves of the composite films measured at 100 and 300 K are shown in Fig. 5. The saturation magnetization values at 100 and 300 K are increased with increasing T_{an}, suggesting that the magnetically ordered region is increased. With increasing T_{an} from 900 to 1100°C, the coercive fields H_C are largely decreased from 209.4 and 60.4 Oe to 110.3 and 39.2 Oe at 100 and 300 K, respectively, which is due to a significant reduction in the grain boundary area of $La_{0.7}Sr_{0.3}Mn_{1+d}O_3$, acting as the domain wall pinning site, because of grain growth. In fact, somewhat larger average grain size of $La_{0.7}Sr_{0.3}Mn_{1+d}O_3$ is observable for the composite sample annealed at 1100

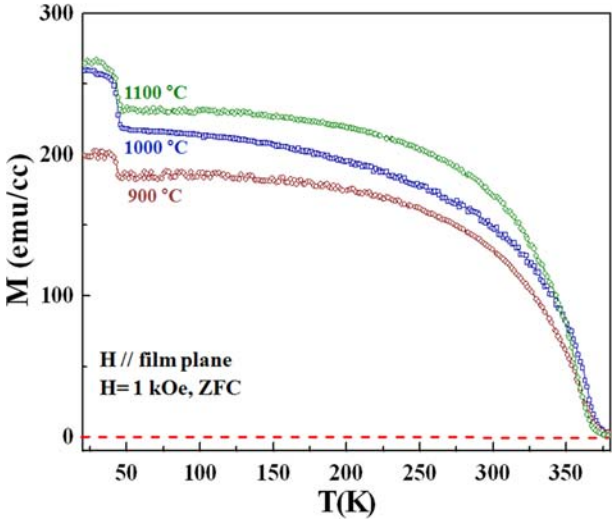

Fig. 4. (Color online) The *M-T* curves of the $La_{0.7}Sr_{0.3}Mn_{1+d}O_3$-$Mn_3O_4$ composite films annealed at the temperature region of 900-1100°C.

°C in Fig. 3 in comparison with that for the composite sample annealed at 1000°C in Fig. 2. Even though the microstructure of the sample annealed at 900°C has not been analyzed yet, the smallest average grain size of $La_{0.7}Sr_{0.3}Mn_{1+d}O_3$ is expected.

The LFMR behaviors of the composite films at 100 and 300 K are shown in Fig. 6(a) and (b), respectively. With increasing T_{an} from 900 to 1100°C, while the LFMR value at 100 K in 1.5 kOe is decreased from 12.2 to 10.4%, the LFMR value at 300 K in 0.5 kOe is increased from 0.76 to 1.29%. On the other hand, with increasing T_{an}, the MR peaks in Fig. 6 commonly become shaper and thus the maximum *d*MR/*dH* values are monotonously increased as listed in the Table 1. The maximum *d*MR/*dH* value of

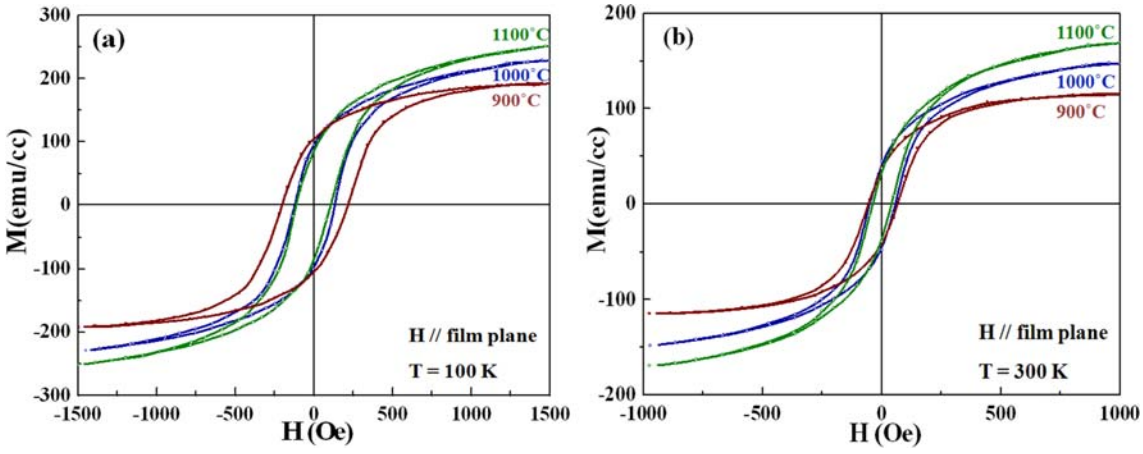

Fig. 5. (Color online) The *M-H* curves of the $La_{0.7}Sr_{0.3}Mn_{1+d}O_3$-$Mn_3O_4$ composite films annealed at the temperature region of 900-1100°C measured at (a) 100 K and (b) 300 K.

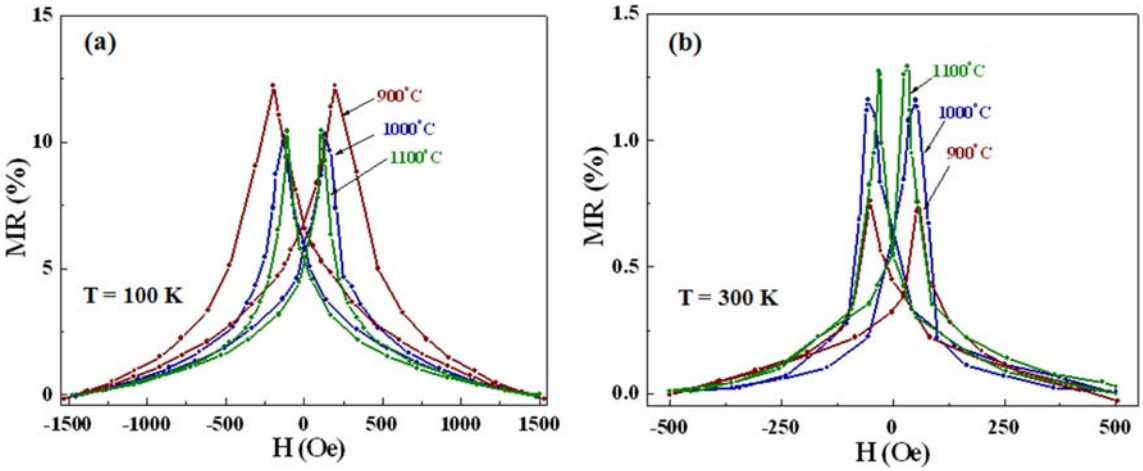

Fig. 6. (Color online) The LFMR behaviors of the $La_{0.7}Sr_{0.3}Mn_{1+d}O_3$-$Mn_3O_4$ composite films annealed at the temperature region of 900-1100°C. The LFMR values were evaluated from the resistivity values at (a) 100 K in the fields up to 1.5 kOe and (b) 300 K in the fields up to 0.5 kOe, respectively.

Table 1. Curie temperature (T_C), resistivity (ρ) and LFMR values of the $La_{0.7}Sr_{0.3}Mn_{1+d}O_3$-$Mn_3O_4$ composite films on *poly*-BZO prepared at three T_{an} values in pure oxygen atmosphere. The data from ref. [13] for the composite bulk with the same composition are also listed for a comparison.

Properties	LSMO-manganese oxide composite bulks (Data from ref. [13])		Composite films on *poly*-BZO: T_{an}(°C)		
	As-sintered (1300°C for 8 h in air)	Post-annealed (850°C for 12 h in pure O_2)	900	1000	1100
T_C (K)	366	366	370	372	368
LFMR (%) at 100 K	8.9	12.9	12.2	10.2	10.4
LFMR (%) at 300 K	1.2	1.7	0.76	1.16	1.29
ρ_{100K} (Ωcm)	0.030	0.030	0.67	0.34	0.51
ρ_{300K} (Ωcm)	0.069	0.068	0.54	0.57	0.91
dMR/dH (%kOe^{-1}) at 300 K	13.2	28.3	9.8	19.6	37.4

37.4%kOe^{-1} at 300 K was achievable from the composite film annealed at 1100°C. Similar to the $La_{0.7}Sr_{0.3}Mn_{1+d}O_3$-$Mn_3O_4$ composite bulk [13], the enhanced LFMR behaviors in the composite films are attributed to a sharp grain boundary effect. The sharp grain boundary effect of $La_{0.7}Sr_{0.3}Mn_{1+d}O_3$ is obviously achievable from the composite film annealed at 1100°C.

The properties of the composite films are summarized in Table 1. For a comparison, properties of the composite bulks before and after the post-annealing from our previous report [13] are also represented. First of all, among the composite films studied here, the highest LFMR value of 1.29% at 300 K in 0.5 kOe was obtainable from the composite film annealed at 1100°C. This LFMR value at 300 K is unprecedentedly high among the LFMR values of LSMO films [24, 26] and LSMO-insulating oxide composite films [19, 25] ever reported. For instance, the LFMR value of 0.7% at room temperature in 0.5 kOe was obtained from a 20 μm-thick $La_{2/3}Sr_{1/3}MnO_3$-CeO_2 composite film deposited by screen printing [19], 1% at 300 K in 0.5 kOe from a 200 nm-thick $(La_{0.75}Sr_{0.25})_{1.05}Mn_{0.95}O_3$ film fabricated by the SPC process [24], 0.7% at 300 K in 0.6 kOe from a 150 nm-thick $La_{2/3}Sr_{1/3}MnO_3$-In_2O_3 composite film deposited by spin coating [25], and 0.9% at room temperature in 0.5 kOe from 150-200 nm-thick $La_{0.71}Sr_{0.29}Mn_{1.01}O_{3-\delta}$ film fabricated by RF magnetron sputtering [26]. Next, compared with the composite bulks, the composite films show around one order of magnitude increase in their resistivity values in Table 1. This increase in resistivity is attributed to a large increase in the grain boundary area because of greatly reduced average grain size of $La_{0.7}Sr_{0.3}Mn_{1+d}O_3$. While the average grain size of $La_{0.7}Sr_{0.3}Mn_{1+d}O_3$ is ~1.3 μm in the composite bulk sintered at 1300°C in air [13], it is ~100 nm in the composite film annealed at 1000°C in Fig. 2. It is also attributed to a reduced percolation path because of refined insulating T-

Mn_3O_4 grains. Finally, as listed in Table 1, since the LFMR value of 1.2% with the maximum *d*MR/*dH* value of 13.2%kOe^{-1} at 300 K for as-sintered bulk sample was increased to 1.7% with the maximum *d*MR/*dH* value of 28.3%kOe^{-1} at 300 K in 0.5 kOe for post-annealed bulk sample [13], a positive post annealing effect is expected also for the composite films.

4. Conclusions

The $La_{0.7}Sr_{0.3}Mn_{1+d}O_3$-$Mn_3O_4$ composite films on *poly*-BZO substrates were prepared by *ex-situ* solid phase crystallization of amorphous films deposited by dc-magnetron sputtering at room temperature. The highest LFMR value of 1.29% at 300 K in 0.5 kOe with the maximum *d*MR/*dH* value of 37.4%kOe^{-1} could be obtained from the composite film on *poly*-BZO substrates annealed at 1100 °C even though this sample possessed high density micro-cracks, which is attributed to effective spin dependent scattering at sharp $La_{0.7}Sr_{0.3}Mn_{1+d}O_3$ grain boundaries. Although the LFMR value of 1.29% at 300 K in 0.5 kOe is unprecedentedly high among the LFMR values of LSMO films and LSMO-insulating oxide composite films ever reported, further improvement may be possible if the problem of micro-cracks is overcome in the composite films.

Acknowledgements

This work was supported by the Korea Science and Engineering Foundation (KOSEF) grant funded by the Korea government (MEST) (No. KRF-0417-20100021). The first author Young-Min Kang is now at Samsung Advanced Institute of Technology.

References

[1] J. M. D. Coey, M. Viret, and S. von Molnar, Adv. Phys. **48**, 167 (1999).
[2] A. M. Haghiri-Gosnet and J. P. Renard, J. Phys. D **36**, R127 (2003).
[3] W. Prellier, P. Lecoeur, and B. Mercey, J. Phys.: Condens. Matter. **13**, R915 (2001).
[4] R. von Helmolt, J. Wecker, B. Holzapfel, L. Schultz, and K. Samwer, Phys. Rev. Lett. **71**, 2331 (1993).
[5] S. Jin, T. H. Tiefel, M. McCormack, R. A. Fastnacht, R. Ramesh, L. H. Chen, Science **264**, 413 (1994).
[6] H. Gencer, M. Pektas, Y. Babur, V. S. Kolat, T. Izgi, and S. Ataly, J. Magnetics **17**, 176 (2012).
[7] H. Y. Hwang, S.-W. Cheong, N. P. Ong, and B. Batlogg, Phys. Rev. Lett. **77**, 2041 (1996).
[8] J.-H. Park, E. Vescovo, H.-J. Kim, C. Kwon, R. Ramesh, and T. Venkatesan, Phys. Rev. Lett. **81**, 1953 (1998).
[9] R. Mahesh, R. Mahendiran, A. K. Raychaudhuri, and C. N. R. Rao, Appl. Phys. Lett. **68**, 2291 (1996).
[10] A. Gupta, G. Q. Gong, Gang Xiao, P. R. Duncombe, P. Lecoeur, P. Trouilloud, Y. Y. Wang V. P. Dravid, and J. Z. Sun, Phys. Rev. B **54**, R15629 (1996).
[11] X. S. Yang, Y. Yang. W. He, C. H. Cheng, and Y. Zhao, J. Phys. D: Appl. Phys. **41**, 115009 (2008).
[12] A. Gaur and G. D. Varma, J. Alloys Compd. **453**, 423 (2008).
[13] Y.-M. Kang, H.-J. Kim, and S.-I. Yoo, Appl. Phys. Lett. **95**, 052510 (2009).
[14] D. K. Petrov, L. Krusin-Elbaum, J. Z. Sun, C. Feild, and P. R. Duncombe, Appl. Phys. Lett. **75**, 995 (1999).
[15] C. Xionga, H. Hu, Y. Xiong, Z. Zhang, H. Pi, X. Wu, L. Li, F. Wei, and C. Zheng, J. Alloys Compd. **479**, 357 (2009).
[16] J. Kumar, R. K. Singh, H. K. Singh, P. K. Siwach, R. Singh, and O. N. Srivastava, J. Alloys Compd. **455**, 289 (2008).
[17] P. Kameli, H. Salamati, and M. Hakimi, J. Alloys Compd. **463**, 18 (2008).
[18] H.-J. Kim and S.-I. Yoo, J. Alloys Compd. **521**, 30 (2012).
[19] S. Valencia. O. Castano, J. Fontcuberta, B. Martinez, and L. Balcells, J. Appl. Phys. **94**, 2524 (2003).
[20] Z. Bi, E. Weal, H. Luo, A. Chen, J. L. MacManus-Driscoll, Q. Jia, and H. Wang, J. Appl. Phys. **109**, 054302 (2011).
[21] L. Yan, L. B. Kong, T. Yang. W. C. Goh, C. Y. Tan, C. K. Ong, M. A. Rahman, T. Osipowicz, and M. Q. Ren, J. Appl. Phys. **96**, 1568 (2004).
[22] S. A. Koster, V. Moshnyaga, K. Samwer, O. I. Lebedev, G. van Tendeloo, O. Shapoval, and A. Belenchuk, Appl. Phys. Lett. **81**, 1648 (2002).
[23] A. Chen, Z. Bi, C. F. Tsai, J. H. Lee, Q. Su, X. Zhang, Q. Jia, J. L. MacManus-Driscoll, and H. Wang, Adv. Funct. Mater. **21**, 2423 (2011).
[24] Y.-M. Kang, A. N. Ulyanov, S. Y. Lee, and S.-I. Yoo, Met. Mater. Int. **17**, 1045 (2011)
[25] I.-B. Shim, B.-W. Lee, and C. S. Kim, J. Magn. Magn. Mater. **239**, 279 (2002).
[26] K.-K. Choi, T. Taniyama, and Y. Yamazaki, J. Appl. Phys. **90**, 6145 (2001).
[27] J. A. M. van Roosmalen, P. van Vlaanderen, and E. H. P. Cordfunke, J. Solid State Chem. **114**, 516 (1995).
[28] Y.-M. Kang, S.-H. Wee, S.-I. Baik, S.-G. Min, S.-C. Yu, S.-H. Moon, Y.-W. Kim, and S.-I. Yoo, J. Appl. Phys. **97**, 10A319 (2005).
[29] Y.-M. Kang, A. N. Ulyanov, and S.-I. Yoo, Phys. Stat. Sol. A **204**, 763 (2007).
[30] A. S Borovick-Ramanov and M. P. Orlova, Sov. Phys. JETP **5**, 1023 (1957).